Metallomics

Accepted Manuscript

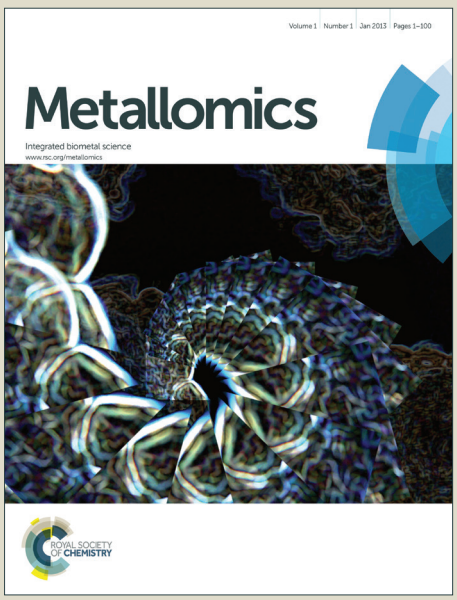

ROYAL SOCIETY OF CHEMISTRY

www.rsc.org/metallomics

Influence of gold-bipyridyl derivants on aggregation and disaggregation of prion neuropeptide PrP106–126

Cong Zhao,[†] Xuesong Wang,[†] Lei He,[†] Dengsen Zhu,[†] Baohuai Wang,[‡]

Weihong Du[†*]

[†]Department of Chemistry, Renmin University of China, Beijing, 100872, China

[‡]College of Chemistry and Molecular Engineering, Peking University, Beijing, 100871, China

Key words: PrP106-126, aggregation, gold-bpy derivant, interaction.

[*]Correspondence. Tel/Fax: 8610-6251-2660/6444, Email: whdu@chem.ruc.edu.cn.

Abstract

Metal complexes can effectively inhibit the aggregation of amyloid peptides, such as Aβ, human islet amyloid polypeptide, and prion neuropeptide PrP106–126. Gold (Au) complexes exhibited better inhibition against PrP106–126 aggregation, particularly Au–bipyridyl (bpy) complex; however, the role of different ligand configurations remains unclear. In the present study, three derivants of Au–bpy complexes, namely, $[Au(Me_2bpy)Cl_2]Cl$, $[Au(t\text{-}Bu_2bpy)Cl_2]Cl$, and $[Au(Ph_2bpy)Cl_2]$-Cl, were investigated to influence the aggregation and disaggregation of PrP106–126. The steric and aromatic effects of the ligand resulted in an enhanced binding affinity. Inhibition was significantly affected by a large ligand. The neurotoxicity of the SH–SY5Y cell induced by PrP106–126 was reduced by the three Au-bpy derivants. However, the disaggregation ability was not in accordance with the results of selected complexes during inhibition, suggesting a different mechanism of interactions between gold complexes and PrP106–126. The key peptide residues contributed to both the inhibition and disaggregation capability through the metal coordination and hydrophobic interaction with the metal complexes. Thus, understanding the aggregation mechanism of the prion peptide would be helpful in designing novel metal-based drugs against amyloid fibril formation.

Introduction

Prion diseases, known as transmissible spongiform encephalopathies (TSEs), are a class of fatal neurodegenerative diseases. Human prion diseases include Creutzfeldt–Jakob disease, Kuru, Gerstmann–Strussler syndrome, and fatal familial insomnia.[1] A suggested pathogenic mechanism of these diseases involves transition from a prion protein normal cellular form (PrP^c), which is rich in α-helix, to a pathogenic scrapie isoform (PrP^{sc}), which is rich in β-sheet.[2] The biological functions of a PrP^c are partly understood, and results showed that PrP^c was involved in cellular signal transduction and metal ion transport processes.[3-9] After PrP^c transitions to PrP^{sc}, PrP aggregates, forms amyloid fibrils, and loses its biological functions with severe neurotoxicity.[10, 11]

The N-terminal prion fragment PrP106–126 (106–KTNMKHMAGAAAAGAV-VGGLG–126) is a common investigation model because this fragment is soluble in water and exhibits several physicochemical and biological properties with PrP^{sc}, such as proteinase K hydrolysis resistance, aggregation in solution, and neurotoxicity.[12-16] A toxicity of PrP106–126 has been thought to be correlated with its primary structure. PrP106–126 is composed of two distinct regions, i.e., a hydrophilic region (K106–M112) and a hydrophobic region (A113–G126). PrP106–126 has high tendency to aggregate into β-sheet structures, form amyloid fibrils in vitro, and become partially resistant to proteolysis.[17, 18] Recent studies have reported that an oligomerization of PrP106–126 is caused by association of ordered β-hairpin monomers rather than disordered monomers.[19, 20] Another study have shown that early

ordered oligomers are stacked by an interface of hydrophobic C-terminal residues (A113–G126), which may increase fibril growth rate and form the fibril structure.[21] The spanning fragment of Asn108–Met109–Lys110–His111–Met112 in PrP106–126 exhibits a "turn-like" conformation, wherein His111 is located before the starting point of an α-helix; the effects of His111 are important in modulating the conformational flexibility and heterogeneity of PrP106–126.[22] A number of experimental data has demonstrated that the side chains of His111 and Met109/112 contribute to a high metal-binding affinity.[23-29]

Studies on prion inhibitors have been reported. Metal ions, such as Cu^{2+}, Zn^{2+}, Mn^{2+}, and Ni^{2+}, bind to prion protein and influence the aggregation of PrP106–126.[23, 24, 27, 28, 30] Some researchers have reported the inhibitory effects of small molecules either on the aggregation behavior or neurotoxicity of PrP106–126.[31-34] For instance, small-stress molecules like tetracycline and carnosine inhibit the aggregation and neurotoxicity of PrP106–126 by preventing protein denaturation and maintaining protein stability.

Metal complexes, especially those from platinum, gold, and ruthenium, exhibit better inhibition against aggregation of PrP106–126 and other amyloid peptides, such as Aβ, α-synuclein, and HIAPP (human islet amyloid polypeptide), through metal coordination and hydrophobic interaction.[35-39] Although these compounds are potential antitumor metallodrugs, their effect against neurodegenerative diseases, such as Alzheimer's and Parkinson's disease, should not be neglected.[40-44]

Au complexes were used to inhibit amyloid formation in PrP106–126.[37, 45] The

existence of different ligands, such as 1,10-phenanthroline (phen), diethylenetriamine (dien), and 2,2'-bipyridine (bpy) may cause Au(III) compound to bind to a peptide and affect peptide aggregation. Among the compounds cited, Au-bpy complex exhibited the most significant inhibition against PrP106–126 aggregation.[37] Based on previous results, the bipyridyl ligand was further modified. In the present study, series of Au complexes from bpy derivants were synthesized to investigate the inhibition and steric and aromatic effects of the bpy ligand on PrP106–126 aggregation (Scheme 1). The Au-bpy derivants influenced the aggregation and disaggregation of PrP106–126 at different degrees. Moreover, the Au complexes reduced the SH–SY5Y cell neurotoxicity induced by PrP106–126; however, their binding affinities and capabilities of disaggregation were also affected because of the advantages and disadvantages caused by modifications. These results would help in understanding the aggregation mechanism of PrP106–126 caused by the interactions between Au complexes and the peptide.

Experimental

Materials

Human prion protein fragment PrP106–126 and its mutant, M109F, were chemically synthesized by SBS Co., Ltd. (Beijing, China). The synthesized PrP106–126 and M109F were purified and identified using high performance-liquid chromatography (HPLC) and mass spectrometry (MS) with more than 95%. Purity of PrP106-126 was also confirmed using ^{1}H nuclear magnetic resonance (NMR)

spectroscopy. Ligands, including 4-4'-dimethyl-2,2'-bipyridyl and 4-4'-diphenyl-2,2'-bipyridyl, were purchased from Sigma–Aldrich Co., Ltd. 4-4'-di-tert-butyl-2,2'-bipyridyl was purchased from TCI Shanghai, Co., Ltd. Au complexes were prepared, as described previously, and stored at 277 K for further use. All of the other reagents were of analytical grade.

Electrospray ionization-mass spectrometry (ESI-MS)

ESI-MS spectra were obtained in positive mode by directly introducing the samples at a flow rate of 3 μL/min in an APEX IV FT-ICR high-resolution mass spectrometer (Bruker, USA) equipped with a conventional ESI source. The working conditions were as follows: end plate electrode voltage, −3500 V; capillary entrance voltage, −4000 V; skimmer voltages, 1 and 30 V; and dry gas temperature, 473 K. The flow rates of the drying and nebulizer gases were set at 12 and 6 L/min, respectively. Data analysis 4.0 software (Bruker) was used to acquire data. Deconvoluted masses were obtained using an integrated deconvolution tool. The peptide sample concentration was 50 μM. An equivalent amount of each Au complex was added to the peptide solution for detection.

NMR spectroscopy

^{1}H NMR experiments were performed on a Bruker Avance 400 MHz spectrometer at 298 K. The solvent used was H_2O containing 10% d_6-DMSO. An equivalent amount of Au complex was added to the peptide solution, and the final

concentration of peptide was 0.5 mM. The pH value was adjusted to 5.8 with either DCl or NaOD. The watergate pulse program with gradients was used to suppress the residual water signal. All NMR data were processed using a Bruker Topspin 2.1 software.

Spectrofluorometric measurements

Steady-state fluorescence measurements of the intrinsic phenylalanine residue were performed at room temperature to compare the binding affinity of Au complexes with PrP106–126. Given that PrP106-126 has no luminescent aromatic residue, the single mutant of PrP106-126, M109F, was selected and used as a model considering other species similarity at this residue position. An excitation wavelength of 260 nm was determined based on a previous report.[46] The dissociation constant (K_d) was calculated from the plot of the fluorescence intensity through the Au complex concentration using Eq. (1):

$$\Delta F = F_0 - F_L = (F_0 - F_\alpha)\{K_d + P_0 + T - [(K_d + P_0 + T)^2 - 4P_0T]^{1/2}\}/2P_0 \qquad (1)$$

where F_0 and F_L are the measured peptide fluorescence intensities at 287 nm in the absence and presence of Au complexes,[47, 48] respectively, and F_α is the maximum quenching of the peptide fluorescence. P_0 refers to the peptide initial concentration and T represents the concentration of added Au complex. The concentration of M109F was 100 μM. The results were obtained from three repeated experiments.

Thioflavin T (ThT) assay

For the inhibition assay, 1 mM of Au complex was added to 1 mM of PrP106–126 in 10 mM phosphate buffer at a pH of 7.2. The mixture was incubated for 24 h. Sample concentration was decreased to 100 μM, and 100 μM of ThT was added to the solution. The resulting solution was monitored using an F-4600 spectrofluorometer (Hitachi Ltd., Japan). The ThT fluorescence signal was measured by determining the average of the fluorescence emissions at 500 nm for 10 s at an excitation of 432 nm. For the IC_{50} determination, the Au complex concentrations used varied from 25 μM to 200 μM. For the disaggregation assay, 1 mM of PrP106–126 was aged for 24 h in a 10 mM of phosphate buffer at a pH of 7.2. The equivalent complex with the peptide was incubated for 24 h. Sample concentration decreased to 100 μM, and 100 μM of ThT was added to the sample. The fluorescence of the mixture was then determined. The reported data were the average of three experiments.

Atomic force microscopy (AFM)

Samples were prepared by adding 1 mM of Au complex to 1 mM of the peptide solution, and the resulting solution was incubated at 310 K for 24 h. The final peptide concentration used in the AFM experiment was 10 μM. Images were obtained using a Veeco D3100 instrument (Veeco Instruments 151, Inc.,) in tapping mode with a silicon tip under ambient conditions. The scanning rate and scanning line employed were 1 Hz and 512, respectively.

MTT assay

Human SH-SY5Y neuroblastoma cells were cultured in a 1:1 mixture of Dulbecco's modified Eagle's medium and F12 medium supplemented with 10% of fetal bovine serum, 2 mM of glutamine, 100 U/mL penicillin, and 100 U/mLstreptomycin. Cell growth was performed in a humidified incubator at 310 K with 95% of air and 5% of CO_2. Cell survival was assessed by measuring the reduction of 3-(4, 5-dimethylthiazol-2-yl)-2,5-diphenyl-terazolium bromide (MTT). Approximately 100 μM of PrP106–126 with or without 100 μM of the Au complex was incubated for 24 h. The mixture was then added to the cells and allowed to react for 4 d. The cells were incubated with 10 μL of MTT at 310 K for 4 h. The absorbance at 570 nm was measured using a UV–vis spectrophotometer. Each experiment was performed four times. Data were calculated as percentage of the untreated control value.

Results

Synthesis of gold-bpy derivants

Three Au complexes, namely, $[Au(Me_2bpy)Cl_2]Cl$, $[Au(t\text{-}Bu_2bpy)Cl_2]Cl$, and $[Au(Ph_2bpy)Cl_2]Cl$, were synthesized based on a previous study.[49] These complexes were identified by NMR (Figure S1). The Au-bpy derivants were synthesized to compare the steric and aromatic effects of the compounds during their inhibition against PrP106–126 aggregation and understand the peptide aggregation mechanism.

ESI-MS spectra of the prion neuropeptide with Au complexes

Equivalent amounts of the Au complex and peptide were incubated to determine whether or not the Au complexes are directly bound to PrP106–126. The final solution was analyzed by ESI-MS. The resulting ESI-MS spectra are shown in Figure 1. The free PrP106–126 exhibited a peak of 956.50 (2+), corresponding to its expected mass. Adding $[Au(Me_2bpy)Cl_2]Cl$, $[Au(t\text{-}Bu_2bpy)Cl_2]Cl$, and $[Au(Ph_2bpy)\text{-}Cl_2]Cl$ produced similar results, wherein an adduct peak of 2109.96 was observed. The peak corresponded to the product of PrP106–126~Au. The peak intensity of the complexes was higher than that of the free PrP106–126, suggesting that complexes exhibited strong binding affinity with the peptide. An increase in mass of 197 compared with the adduct peak matched that of the Au(III) ion, indicating the absence of the ligand in the ESI-MS spectrum. This result was similar to that obtained for the $[Au(bpy)Cl_2]PF_6$ complex; the action of metal coordination was supported by the result.[37] Although the adduct had no ligand, the role of the ligand in binding should not be overlooked. The side chain of Met was not oxidized to sulfoxide because the peaks added by 32 or 16 were not found.

$[Au(Ph_2bpy)Cl_2]Cl$ was used as an example to study the dependence of the binding affinity on pH. The ESI-MS experiments conducted at different pH values showed significant differences (Figure S2). The peak of the PrP106-126~Au complex was stronger than that of the free PrP106–126 at pH 3.8. However, the peak of PrP106–126 increased at a pH of 5.8 compared with that of the adduct peak of the PrP106–126~Au complex. At pH 7.0, the peak of PrP106–126 further increased. A

decrease in the binding affinity is associated with increasing pH.

^{1}H NMR studies on the interaction of the Au complex with PrP106–126

The ^{1}H NMR spectrum of PrP106–126 was obtained at a pH value of 5.8 and at 298 K based on a previous study, wherein the characteristic peaks from the side chains of His111 and Met109/112 were identified.[23, 50] After incubating the [Au(Me$_2$bpy)Cl$_2$]Cl, [Au(t-Bu$_2$bpy)Cl$_2$]Cl, or [Au(Ph$_2$bpy)Cl$_2$]Cl with the peptide, the resonance peak of His111 C_δHs shifted from 7.08 ppm to 7.24 ppm with a decrease in intensity. The specific resonance of Met C_εHs at 2.08 ppm also decreased, indicating that the binding sites for [Au(Me$_2$bpy)Cl$_2$]Cl, [Au(t-Bu$_2$bpy)Cl$_2$]Cl and [Au(Ph$_2$bpy)-Cl$_2$]Cl included His111 and Met109/112 (Figure 2). The effects of the three complexes on the peptide NMR spectrum were very similar, with remarkable change occurring at residues His111 and Met109/112, indicating a consistent binding mode of gold complexes to the peptide by metal coordination predominantly.

Moreover, when comparing the downfield NMR portion of the compound with the peptide-mixed system, the peaks from the compound obviously decreased because of the change of their relaxation properties. These signals were from the metal complex but not from free ligand (data not shown), as indicated by their different chemical shifts. The result showed that hydrophobic interaction existed between the ligand and the peptide (Figure S3, S4, and S5).

Binding affinity between the Au complexes and M109F

The method of intrinsic fluorescence quenching was utilized in several studies to calculate K_d and compare binding affinities.[51] Peptides with phenylalanine, tyrosine, and tryptophan residues exhibit intrinsic fluorescence, and the quenching of intrinsic fluorescence represent changes in peptide conformation and its binding ability. PrP106–126 had no aromatic residues; thus, M109F, the single mutant peptide of PrP106–126, was used in this study to investigate similarities in the residue property at this position compared with other PrP species. The residue Met112 is more important than Met109 and left for the binding of complex to peptide.

The fluorescence intensity of the peptide M109F at 287 nm in the presence of a Au complex was used to estimate K_d by a nonlinear least-square regression using Eq. (1). The calculated K_d of $[Au(Me_2bpy)Cl_2]Cl$, $[Au(t\text{-}Bu_2bpy)Cl_2]Cl$, and $[Au(Ph_2\text{-}bpy)Cl_2]Cl$ in M109F were $4.3 \pm 1.5 \times 10^{-6}$ M, $9.7 \pm 2.1 \times 10^{-6}$ M, and $3.5 \pm 1.5 \times 10^{-7}$ M, respectively (Figure 3). The K_d values showed that the peptides exhibited high binding affinity with the gold complexes; however, the K_d values for M109F were not equal to that of PrP106–126.

ThT analysis of the PrP106–126 aggregation inhibited by Au complexes

Studies on the inhibition of peptide aggregation by complexes are vital because aggregation was related to cellular neurotoxicity.[52] As reported in previous studies, PrP106–126 aggregation was monitored using the fluorescence dye ThT. When ThT was bound to an amyloid peptide, an excitation at 432 nm and a strong emission at 500 nm were observed.[53] The control experiment was performed to prevent the

influence of gold complex on ThT. The gold complexes did not exhibit an absorption at 500 nm in the UV spectrum, and the inner filter effect of ThT fluorescence on the complexes was not observed. Figure 4 shows the changes in the ThT fluorescence when gold complexes were added to the peptide PrP106–126. The decrease in ThT fluorescence intensity suggested that fibril formation occurred because of PrP106–126 self-aggregation was inhibited, and the effect on fibril formation was concentration-dependent.

Among the Au complexes used, $[Au(Ph_2bpy)Cl_2]Cl$ showed the strongest inhibitory effect on PrP106–126 aggregation; its IC_{50} value was 61.99 ± 3.15 μM. By comparison, $[Au(Me_2bpy)Cl_2]Cl$ and $[Au(t\text{-}Bu_2bpy)Cl_2]Cl$ exhibited similar inhibitory effect that was relatively weaker than that of $[Au(Ph_2bpy)Cl_2]Cl$; their IC_{50} values were 67.99 ± 6.01 and 68.54 ± 6.54 μM, respectively. The IC_{50} value of $[Au(bpy)Cl_2]PF_6$ was 76.06 ± 8.49 μM (Figure S6). The weaker effect of $[Au(bpy)Cl_2]PF_6$ suggested that adding gold-bpy derivants modified the inhibition of peptide aggregation.

Morphology of the prion-neuropeptide aggregation

AFM was performed to determine the effect of the Au-bpy derivants on peptide aggregation and fibril formation. The thick-fibrillar structure of the PrP106–126 after 24 h of incubation at 310 K suggested a strong aggregation state (Figure 5A). However, the AFM images of PrP106–126 with Au complexes showed that the fibril formation was inhibited. $[Au(Ph_2bpy)Cl_2]Cl$ exhibited the strongest inhibition against

PrP106–126 aggregation (Figure 5D) compared with [Au(Me_2bpy)Cl_2]Cl and [Au(t-Bu_2bpy)Cl_2]Cl (Figures 5B and 5C, respectively). Few fibrils formed in the [Au(Ph_2bpy)Cl_2]Cl and PrP106-126 system, whereas short hair-like filaments were observed in the other two systems. The results of the AFM images were in agreement with those of the ThT assay.

PrP106–126 disaggregation induced by Au complexes

Inhibition against peptide aggregation is an important property that potential metallodrugs should exhibit. This property is necessary because it prevents the formation of toxic species. However, existing amyloid fibrils also need to be disaggregated. Tanshinones were used to prevent and disaggregate Aβ peptide.[54] Unfortunately, not all inhibitors of amyloid formation have disaggregation ability, such as nordihydroguaiaretic acid, which is an Aβ inhibitor.[55] ThT assay and AFM experiments were performed to determine the disaggregation caused by selected Au-bpy derivants. (Figure 6). [Au(Ph_2bpy)Cl_2]Cl showed weaker disaggregation with PrP106–126, which are contrary to the inhibition results. [Au(bpy)Cl_2]PF_6 exhibited a satisfactory disaggregation ability, whereas [Au(Me_2bpy)Cl_2]Cl and [Au(t-Bu_2bpy)-Cl_2]Cl showed results similar to their inhibition behavior. The AFM images were in accordance with the disaggregation results of the ThT assay, as shown in Figure 7. The PrP106–126 and Au complex with a ratio of 1:3 produced short hair-like filaments that were observed in PrP106–126 after it was treated with [Au(bpy)Cl_2]PF_6. Long fibrils were found after the peptide was treated with [Au(Ph_2bpy)Cl_2]Cl.

Interaction difference between peptide inhibition and disaggregation occurred.

Neurotoxicity of the PrP106–126 regulated by Au complexes

Au complexes interacted with PrP106–126, preventing the aggregation of PrP106–126. The ability of Au complexes to reduce the neurotoxicity of PrP106–126 was assessed using human SH–SY5Y neuroblastoma cells. Cell survival was evaluated after treating the SH–SY5Y cells with peptide or with peptide and Au complex. Compared with the control sample, cell viability decreased to 36% for the cells treated with PrP106–126, as measured by the MTT assay. The Au complexes exhibited toxicity to SH–SY5Y cells (Figure S7). Adding Au complexes to PrP106–126 decreased cell cytotoxicity, a behavior induced by PrP106–126; the cell viability increased to 63% for $[Au(Me_2bpy)Cl_2]Cl$, 68% for $[Au(t\text{-}Bu_2bpy)Cl_2]Cl$, and 61% for $[Au(Ph_2bpy)Cl_2]Cl$ (Figure 8). The three complexes prevented the cytotoxicity induced by PrP106–126.

Discussion

Binding affinity of Au complexes with the prion peptide

The Au-bpy derivants used in this study exhibited high binding affinity to PrP106–126 and its mutant M109F. As shown in the ESI-MS spectrum, the dominant adduct peak was the PrP106–126~Au complex for all of the three complexes that formed. This result indicates that metal coordination was the major binding mode of the complexes. Compared with Au^{3+} ion, the existence of a ligand induced a specific

binding of the Au(III) complexes and the peptide.[37] What's more, after incubating metal complex with the peptide, the resonance peaks from the complex didn't shift but obviously decreased in the downfield NMR region, indicating that the ligand interacts with the peptide, changes the conformation of the peptide and further inhibits peptide aggregation as a part of the complex. Taking results of ESI-MS and NMR in consideration, PrP106–126~Au-ligand should exist in solution though it was not directly detected by ESI-MS. Despite the fact that many metal complexes may undergo hydrolysis in solution, this occurrence did not affect the binding specificity of the complexes to the peptide.

Furthermore, the pH-dependent binding affinity of the $[Au(Ph_2bpy)Cl_2]Cl$ showed an important effect of the ligand. Increasing the pH from 3.8 to 7.0 caused the $[Au(Ph_2bpy)Cl_2]Cl$ to hydrolyze in solution. A decrease in the binding affinity was observed because of the decrease in the adduct peak intensity. Only the PrP106–126~Au complex was observed in the MS spectra because the interaction between the ligand and the peptide or the interaction between the Au(III) and the peptide weakened the Au(III)–ligand bonds.

Interestingly, the results of intrinsic fluorescence quenching showed that the binding affinity of the $[Au(Me_2bpy)Cl_2]Cl$ was higher than that of the $[Au(t\text{-}Bu_2bpy)Cl_2]Cl$. This behavior was induced by the greater steric effect of the $t\text{-}Bu_2bpy$ ligand. In addition, $[Au(Ph_2bpy)Cl_2]Cl$ exhibited the highest binding affinity compared with $[Au(Me_2bpy)Cl_2]Cl$ and $[Au(t\text{-}Bu_2bpy)Cl_2]Cl$. The mutation of Met109 may change one potential binding site and add an aromatic amino acid into

the system if the peptide M109F is considered. The disadvantage of a large steric effect of Ph_2bpy on binding was overcome by the advantage of the aromatic and hydrophobic effects between the Ph_2bpy ligand and the Phe residue. As a result, the Au complexes exhibited high binding affinity to the prion peptide during metal coordination; hydrophobic interaction between the ligand and the peptide also occurred.

Function of the ligands during its interaction with PrP106–126

The existence of ligands induced a specific binding of Au complexes with the peptide and affected its aggregation and disaggregation. Comparing the $[Au(bpy)Cl_2]PF_6$, $[Au(Me_2bpy)Cl_2]Cl$, $[Au(t\text{-}Bu_2bpy)Cl_2]Cl$, and $[Au(Ph_2bpy)Cl_2]Cl$, the ligand steric effects are in a larger order. The large steric effect was unfavorable to the binding of Au complexes and peptides, but may cause positive effects during inhibition because a large steric effect prevented the peptide from forming a specific secondary structure and further aggregation. The bpy ligand exhibited strong steric and aromatic effects; hence, the modification of Me_2bpy and $t\text{-}Bu_2bpy$ caused minor enhancement in steric effect. As a result, $[Au(Me_2bpy)Cl_2]Cl$ and $[Au(t\text{-}Bu_2bpy)\text{-}Cl_2]Cl$ exhibited similar experimental results in the ThT assay and the AFM images. However, the $[Au(Ph_2bpy)Cl_2]Cl$ had two phenyl groups; thus, hydrophobic and aromatic effects of the ion improved significantly. These effects exhibited a major function in the complex–peptide interaction. Therefore, the $[Au(Me_2bpy)Cl_2]Cl$ and $[Au(t\text{-}Bu_2bpy)Cl_2]Cl$ exhibited a similar inhibitory ability in the ThT assay of

inhibition, which was stronger than that of the [Au(bpy)Cl_2] PF_6, but weaker than that of the [Au(Ph_2bpy)Cl_2]Cl.

The steric effect exhibited a major role in the disaggregation process because of the highly fibrotic peptide structure. The [Au(bpy)Cl_2] PF_6 exhibited an advantage over the other complexes because Au complexes with smaller ligands caused better peptide disaggregation, as observed in the ThT assay of disaggregation. Under the condition of a mature fibril formation, the folded structure of PrP106–126 was not suitable for binding with Au complexes as in random coil structure.

Differences between the aggregation and disaggregation process

The three Au(III)-bpy derivants exhibited better inhibition on PrP106–126 aggregation, as observed in the ThT assay and the AFM images. Having the same central cation, the complexes exhibited similar binding mode to the peptide. However, the inhibitory effects among them were not equal because of differences in their molecular configurations. The [Au(Ph_2bpy)Cl_2]Cl complex exhibited the most significant inhibition among the three compounds used. The lowest IC_{50} value of this compound was 61.99 μM. This result showed that large steric and aromatic effects were beneficial in inhibition.

By contrast, the complex [Au(bpy)Cl_2]PF_6 exhibited the best disaggregation ability, while [Au(Ph_2bpy)Cl_2]Cl exhibited the weakest disaggregation. Considering different motivational and experimental processes between inhibition and disaggregation, the binding affinity of the compound [Au(Ph_2bpy)Cl_2]Cl was affected

by peptide pre-aggregation. The presence of large ligands in this compound may cause unfavorable dispersion of the mature aggregates. His111 and Met109/112 were the potential sites for the binding of the Au(III) complex and PrP106–126. The aggregation of the peptide concealed the potential binding sites at larger extents than that in the inhibition process, which allow direct binding of the complex to the peptide. This behavior indicates the importance of these residues during the aggregation of the prion neuropeptide. The aggregation mechanism of the amyloid peptide to form a β-sheet conformation, wherein His111 is located at an important position, should be understood. Mature fibrils may prevent the hydrophobic interaction between large ligands and peptides.

Influence factors in the disaggregation of the PrP106–126

The prion neuropeptide PrP106–126 can self-aggregate and form amyloid fibrils through a transition of the β-sheet, oligomers, and profibrils; this characteristic is exhibited by other amyloid peptides.[20, 21, 56-60] L-type folding and β-hairpin conformation existed during oligomerization and fibril formation.[20, 21] The turn-like fragment of the Asn108–Met112 and the residue His111 played a crucial role in their aggregation and binding affinity to other molecules in whatever process they undergo. The difference between the inhibition and disaggregation results, as observed in the ThT assay and AFM images of Au-bpy derivants, confirmed that key residues contributed to both aggregation and resistance of disaggregation. Mature fibril surfaces should be wrapped by hydrophobic peptide side chains that resist the binding

of a metal complex with a large ligand. This characteristic indicates a decreased steric interaction and consequent weak metal binding. Efficient disaggregation did not only require high metal binding, but also adequate hydrophobic interaction. Therefore, ligands should be designed to disperse mature fibrils, which is a critical factor in potential metallodrug development.

Neurotoxicity of the PrP106-126 impaired by Au complexes

Human SH–SY5Y cells that were treated with PrP106–126 exhibited a concentration- and time-dependent decrease in the number of active cells. In the present study, the SH–SY5Y cell viability that was induced by PrP106–126 after a 4 d treatment decreased to 36%. Under the same incubation conditions, adding Au complexes prevented the neurotoxicity of PrP106–126 by about 30%. Considering the cytotoxicity of Au complexes (Figure S7), these complexes reduced the neurotoxicity of PrP106–126 by half. Adding Au complexes to PrP106–126 reduced PrP106–126 toxicity; the cell viabilities for $[Au(bpy)Cl_2]PF_6$, $[Au(Me_2bpy)Cl_2]Cl$, $[Au(t\text{-}Bu_2bpy)\text{-}Cl_2]Cl$, and $[Au(Ph_2bpy)Cl_2]Cl$ increased to 65%, 63%, 68%, and 61%, respectively. The complexes exhibited better regulatory ability on the neurotoxicity of PrP106–126, implying their potential application as prion disease inhibitors.

Briefly, the present study showed that modifying the bpy ligand influenced the interaction between Au complexes and PrP106–126 on both inhibition and disaggregation process. The difference between steric and aromatic effects resulted in different binding affinities and inhibitory effects. The inhibitory effects were

enhanced by modification, and neurotoxicities were prevented. The three Au-bpy derivants exhibited different results during the inhibition and disaggregation processes, suggesting distinct mechanism of interactions between the Au complexes and the PrP106–126 in different processes. Further modifications should be performed to improve the disaggregation ability, and identify the peptide–complex structure. This study is valuable in understanding the aggregation mechanism of prion peptides that are affected by Au complexes. The results of this study may be used to develop novel metal-based drugs against amyloid fibril formation.

Acknowledgements

This work was supported by the National Natural Science Foundation of China (No. 21271185, and No. 21473251), and the National Basic Research Program (No. 2011CB808503).

References

1. S. B. Prusiner, *Science*, 1997, **278**, 245-251.
2. S. B. Prusiner, *Proc. Natl. Acad. Sci. U. S. A.*, 1998, **95**, 13363-13383.
3. J. Collinge, M. A. Whittington, K. C. L. Sidle, C. J. Smith, M. S. Palmer, A. R. Clarke and J. G. R. Jefferys, *Nature*, 1994, **370**, 295-297.
4. J. R. Criado, M. Sanchez-Alavez, B. Conti, J. L. Giacchino, D. N. Wills, S. J. Henriksen, R. Race, J. C. Manson, B. Chesebro and M. B. A. Oldstone, *Neurobiol. Dis.*, 2005, **19**, 255-265.
5. M. H. Lopes, G. N. M. Hajj, A. G. Muras, G. L. Mancini, R. M. P. S. Castro, K. C. B. Ribeiro, R. R. Brentani, R. Linden and V. R. Martins, *J. Neurosci.*, 2005, **25**, 11330-11339.
6. O. Milhavet and S. Lehmann, *Brain Res. Rev.*, 2002, **38**, 328-339.
7. G. L. Millhauser, *Annu. Rev. Phys. Chem.*, 2007, **58**, 299-320.
8. N. Vassallo and J. Herms, *J. Neurochem.*, 2003, **86**, 538-544.
9. N. T. Watt, M. N. Routledge, C. P. Wild and N. M. Hooper, *Free Radical Biol. Med.*, 2007, **43**, 959-967.
10. A. Aguzzi, F. Baumann and J. Bremer, *Annu. Rev. Neurosci.*, 2008, **31**, 439-477.
11. P. Stanczak and H. Kozlowski, *Biochem. Bioph. Res. Co.*, 2007, **352**, 198-202.
12. D. R. Brown, *Biochem. J.*, 2000, **352 Pt 2**, 511-518.
13. D. R. Brown, B. Schmidt and H. A. Kretzschmar, *Nature*, 1996, **380**, 345-347.
14. M. Salmona, P. Malesani, L. De Gioia, S. Gorla, M. Bruschi, A. Molinari, F. Della Vedova, B. Pedrotti, M. A. Marrari, T. Awan, O. Bugiani, G. Forloni and F. Tagliavini, *Biochem. J.*, 1999, **342**, 207-214.
15. S. Vilches, C. Vergara, O. Nicolas, G. Sanclimens, S. Merino, S. Varon, G. A. Acosta, F. Albericio, M. Royo, J. A. Del Rio and R. Gavin, *Plos One*, 2013, **8**.
16. P. Walsh, K. Simonetti and S. Sharpe, *Structure*, 2009, **17**, 417-426.
17. D. L. Rymer and T. A. Good, *J. Neurochem.*, 2000, **75**, 2536-2545.
18. C. Selvaggini, L. Degioia, L. Cantu, E. Ghibaudi, L. Diomede, F. Passerini, G. Forloni, O. Bugiani, F. Tagliavini and M. Salmona, *Biochem. Bioph. Res. Co.*, 1993, **194**, 1380-1386.
19. F. Chiti and C. M. Dobson, *Annu. Rev. Biochem.*, 2006, **75**, 333-366.
20. M. Grabenauer, C. Wu, P. Soto, J. E. Shea and M. T. Bowers, *J. Am. Chem. Soc.*, 2010, **132**, 532-539.
21. P. Walsh, P. Neudecker and S. Sharpe, *J. Am. Chem. Soc.*, 2010, **132**, 7684-7695.
22. E. Ragg, F. Tagliavini, P. Malesani, L. Monticelli, O. Bugiani, G. Forloni and M. Salmona, *Eur. J. Biochem.*, 1999, **266**, 1192-1201.
23. E. Gaggelli, F. Bernardi, E. Molteni, R. Pogni, D. Valensin, G. Valensin, M. Remelli, M. Luczkowski and H. Kozlowski, *J. Am. Chem. Soc.*, 2005, **127**, 996-1006.
24. M. F. Jobling, X. Huang, L. R. Stewart, K. J. Barnham, C. Curtain, I. Volitakis, M. Perugini, A. R. White, R. A. Cherny, C. L. Masters, C. J. Barrow, S. J.

Collins, A. I. Bush and R. Cappai, *Biochemistry*, 2001, **40**, 8073-8084.
25. H. J.-K. Kozlowski, A.; Brasun, J.; Gaggelli, E.; Valensin,D.; Valensin, G. Coordin., *Chem. Rev*, 2009, **253**, 2665–2685.
26. E. M. Marcotte and D. Eisenberg, *Biochemistry*, 1999, **38**, 667-676.
27. I. Turi, C. Kallay, D. Szikszai, G. Pappalardo, G. Di Natale, P. De Bona, E. Rizzarelli and I. Sovago, *J. Inorg. Biochem.*, 2010, **104**, 885-891.
28. D. Valensin, K. Gajda, E. Gralka, G. Valensin, W. Kamysz and H. Kozlowski, *J. Inorg. Biochem.*, 2010, **104**, 71-78.
29. W. Q. Zou, J. Langeveld, X. Z. Xiao, S. G. Chen, P. L. McGeer, J. Yuan, M. C. Payne, H. E. Kang, J. McGeehan, M. S. Sy, N. S. Greenspan, D. Kaplan, G. X. Wang, P. Parchi, E. Hoover, G. Kneale, G. Telling, W. K. Surewicz, Q. Z. Kong and J. P. Guo, *J. Biol. Chem.*, 2010, **285**, 13874-13884.
30. B. Belosi, E. Gaggelli, R. Guerrini, H. Kozlowski, M. Luczkowski, F. M. Mancini, M. Remelli, D. Valensin and G. Valensin, *Chembiochem*, 2004, **5**, 349-359.
31. U. Cosentino, D. Pitea, G. Moro, G. A. A. Saracino, P. Caria, R. M. Vari, L. Colombo, G. Forloni, F. Tagliavini and M. Salmona, *J. Mol. Model.*, 2008, **14**, 987-994.
32. M. Kanapathipillai, S. H. Ku, K. Girigoswami and C. B. Park, *Biochem. Bioph. Res. Co.*, 2008, **365**, 808-813.
33. M. Kawahara, H. Koyama, T. Nagata and Y. Sadakane, *Metallomics*, 2011, **3**, 726-734.
34. T. Pillot, L. Lins, M. Goethals, B. Vanloo, J. Baert, J. Vandekerckhove, M. Rosseneu and R. Brasseur, *J. Mol. Biol.*, 1997, **274**, 381-393.
35. G. L. Ma, F. Huang, X. W. Pu, L. Y. Jia, T. Jiang, L. Z. Li and Y. Z. Liu, *Chem. Euro. J.*, 2011, **17**, 11657-11666.
36. L. He, X. S. Wang, C. Zhao, H. F. Wang and W. H. Du, *Metallomics*, 2013, **5**, 1599-1603.
37. Y. Wang, J. Xu, L. Wang, B. Zhang and W. Du, *Chem. Eur. J.*, 2010, **16**, 13339-13342.
38. N. P. Cook, K. Kilpatrick, L. Segatori and A. A. Marti, *J. Am. Chem. Soc.*, 2012, **134**, 20776-20782.
39. F. T. Senguen, N. R. Lee, X. F. Gu, D. M. Ryan, T. M. Doran, E. A. Anderson and B. L. Nilsson, *Mol. Biosyst.*, 2011, **7**, 486-496.
40. K. J. Barnham, V. B. Kenche, G. D. Ciccotosto, D. P. Smith, D. J. Tew, X. Liu, K. Perez, G. A. Cranston, T. J. Johanssen, I. Volitakis, A. I. Bush, C. L. Masters, A. R. White, J. P. Smith, R. A. Cherny and R. Cappai, *Proc. Natl. Acad. Sci. U. S. A.*, 2008, **105**, 6813-6818.
41. A. Casini and J. Reedijk, *Chem. Sci.*, 2012, **3**, 3135-3144.
42. E. Gao, M. C. Zhu, L. Liu, Y. Huang, L. Wang, C. Y. Shi, W. Z. Zhang and Y. G. Sun, *Inorg. Chem.*, 2010, **49**, 3261-3270.
43. H. S. Mansuri-Torshizi, T. S.; Chavan, S. J.; Chitnis,M. P., *J. Inorg. Biochem.*, 1992, **48**, 63–70.
44. S. Padhye, Z. Afrasiabi, E. Sinn, J. Fok, K. Mehta and N. Rath, *Inorg. Chem.*,

2005, **44**, 1154-1156.
45. X. S. Wang, L. He, C. Zhao, W. H. Du and J. Lin, *J. Biol. Inorg. Chem.*, 2013, **18**, 767-778.
46. W. S. VanScyoc, B. R. Sorensen, E. Rusinova, W. R. Laws, J. B. A. Ross and M. A. Shea, *Biophys. J.*, 2002, **83**, 2767-2780.
47. D. L. Jiang, X. J. Li, R. Williams, S. Patel, L. J. Men, Y. S. Wang and F. M. Zhou, *Biochemistry*, 2009, **48**, 7939-7947.
48. L. Ronga, E. Langella, P. Palladino, D. Marasco, B. Tizzano, M. Saviano, C. Pedone, R. Improta and M. Ruvo, *Proteins*, 2007, **66**, 707-715.
49. P. M. V. Ivanov M A, Balashev K P., *Russ. J. Gen. Chem.*, 2003, **73**, 1821-1822.
50. X. S. Wang, B. B. Zhang, C. Zhao, Y. L. Wang, L. He, M. H. Cui, X. T. Zhu and W. H. Du, *J. Inorg. Biochem.*, 2013, **128**, 1-10.
51. R. Perez-Pineiro, T. C. Bjorndahl, M. V. Berjanskii, D. Hau, L. Li, A. Huang, R. Lee, E. Gibbs, C. Ladner, Y. W. Dong, A. Abera, N. R. Cashman and D. S. Wishart, *Febs J.*, 2011, **278**, 4002-4014.
52. K. N. Frankenfield, E. T. Powers and J. W. Kelly, *Protein Sci.*, 2005, **14**, 2154-2166.
53. T. Florio, D. Paludi, V. Villa, D. R. Principe, A. Corsaro, E. Millo, G. Damonte, C. D'Arrigo, C. Russo, G. Schettini and A. Aceto, *J. Neurochem.*, 2003, **85**, 62-72.
54. Q. M. Wang, X. Yu, K. Patal, R. D. Hu, S. Chuang, G. Zhang and J. Zheng, *ACS Chem. Neurosci.*, 2013, **4**, 1004-1015.
55. M. A. Moss, N. H. Varvel, M. R. Nichols, D. K. Reed and T. L. Rosenberry, *Mol. Pharmacol.*, 2004, **66**, 592-600.
56. M. Bartolini, C. Bertucci, M. L. Bolognesi, A. Cavalli, C. Melchiorre and V. Andrisano, *Chembiochem*, 2007, **8**, 2152-2161.
57. R. Kayed, E. Head, J. L. Thompson, T. M. McIntire, S. C. Milton, C. W. Cotman and C. G. Glabe, *Science*, 2003, **300**, 486-489.
58. A. A. Reinke and J. E. Gestwicki, *Chem. Biol. Drug Des.*, 2011, **77**, 399-411.
59. R. Soong, J. R. Brender, P. M. Macdonald and A. Ramamoorthy, *J. Am. Chem. Soc.*, 2009, **131**, 7079-7085.
60. M. Mompean, C. Gonzalez, E. Lomba and D. V. Laurents, *J. Phys. Chem. B*, 2014, **118**, 7312-7316.

Figure Legends

Scheme 1. The molecular structures of [Au(Me_2bpy)Cl_2]Cl (A), [Au(t-Bu_2bpy)Cl_2]Cl (B) and [Au(Ph_2bpy)Cl_2]Cl (C).

Figure 1. ESI-MS spectra of 50 μM PrP106–126 in the presence of equivalent amounts of [Au(Me_2bpy)Cl_2]Cl (A), [Au(t-Bu_2bpy)Cl_2]Cl (B) and [Au(Ph_2bpy)Cl_2] Cl (C).

Figure 2. ^{1}H NMR spectra of 0.5 mM PrP106-126 in 9:1 H_2O/d_6-DMSO solvent at pH 5.8, 298 K. PrP106-126 alone (A), and PrP106-126 in the presence of equivalent amounts of [Au(Me_2bpy)Cl_2]Cl (B), [Au(t-Bu_2bpy)Cl_2]Cl (C) and [Au(Ph_2bpy)Cl_2]Cl (D). The peak marked by triangle was from a C_εHs group of Met109/112 and the peak marked by asterisk was from the C_δHs of His111.

Figure 3. The intrinsic fluorescence titration of peptide M109F by [Au(Me_2bpy)Cl_2]-Cl (black), [Au(t-Bu_2bpy)Cl_2]Cl (red) and [Au(Ph_2bpy)Cl_2]Cl (green). The concentration of the peptide was 100 μM.

Figure 4. The abilities of metal complexes [Au(bpy)Cl_2]PF_6 (blue), [Au(Me_2bpy)-Cl_2]Cl (black), [Au(t-Bu_2bpy)Cl_2]Cl (red) and [Au(Ph_2bpy)Cl_2]Cl (green) to inhibit aggregation of 100 μM PrP106–126 (purple) measured by ThT assay.

Figure 5. Atomic force microscopy images of 10 μM PrP106–126 in the absence (A) and presence of equivalent amounts of [Au(Me_2bpy)Cl_2]Cl (B), [Au(t-Bu_2bpy)Cl_2]Cl (C) and [Au(Ph_2bpy)Cl_2]Cl (D). The scale bar is 500nm.

Figure 6. The abilities of metal complexes [Au(bpy)Cl_2]PF_6 (blue), [Au(Me_2bpy)-

Cl_2]Cl (black), [Au(t-Bu_2bpy)Cl_2]Cl (red) and [Au(Ph_2bpy)Cl_2]Cl (green) to disaggregate fibrils of 100 μM PrP106–126 (purple) measured by ThT assay.

Figure 7. Atomic force microscopy images of 10 μM PrP106–126 disaggregation in the absence (A) and presence of triple amount of [Au(bpy)Cl_2]PF_6 (B), and [Au(Ph_2bpy)Cl_2]Cl (C). The scale bar is 500nm.

Figure 8. The neurotoxicity of PrP106–126 inhibited by gold complexes. The data represented the average of four experiments determined by MTT assay.

TOC Comment

Gold-bipyridyl derivants affect aggregation and disaggregation of prion neuropeptide PrP106–126

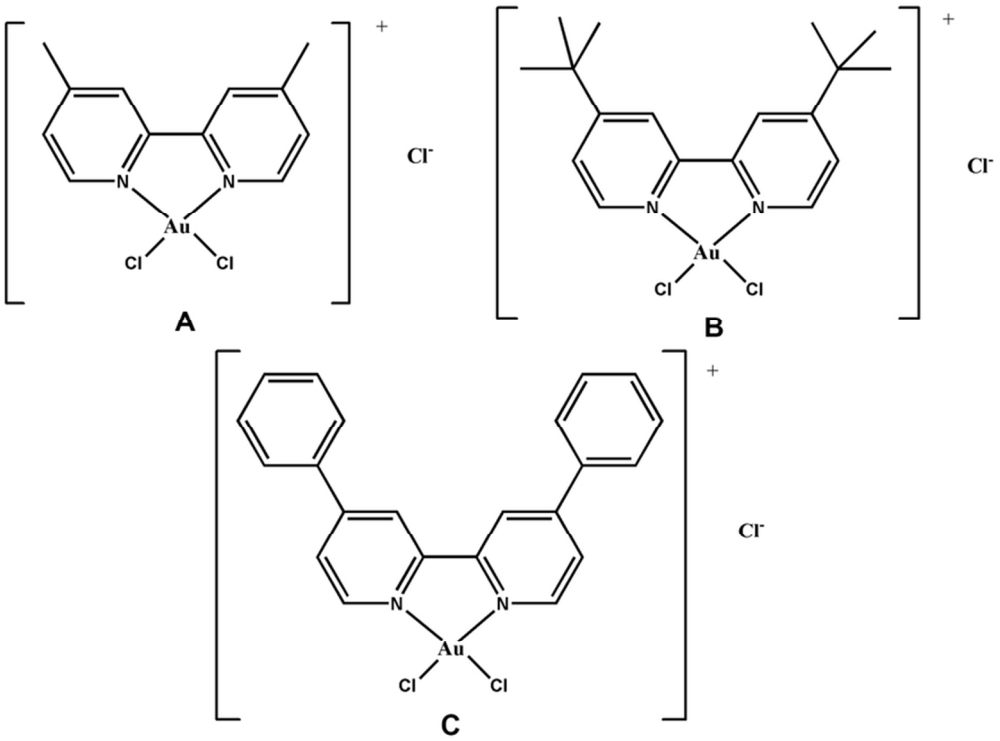

75x56mm (300 x 300 DPI)

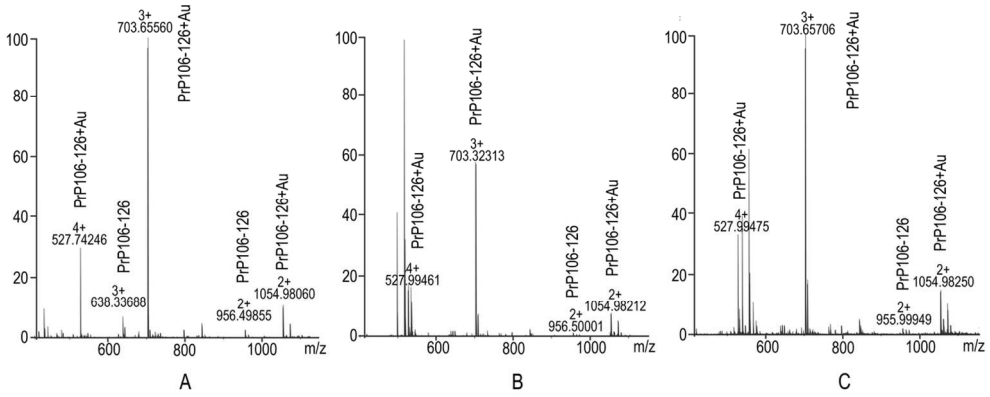

121x49mm (300 x 300 DPI)

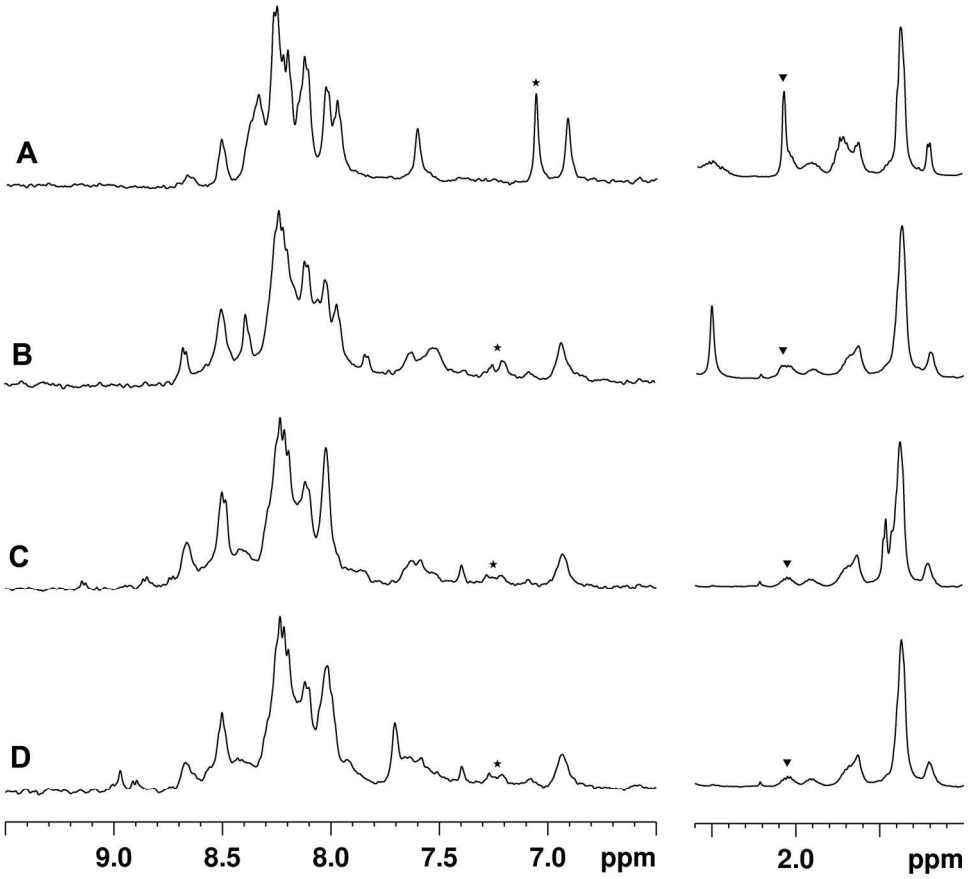

190x171mm (300 x 300 DPI)

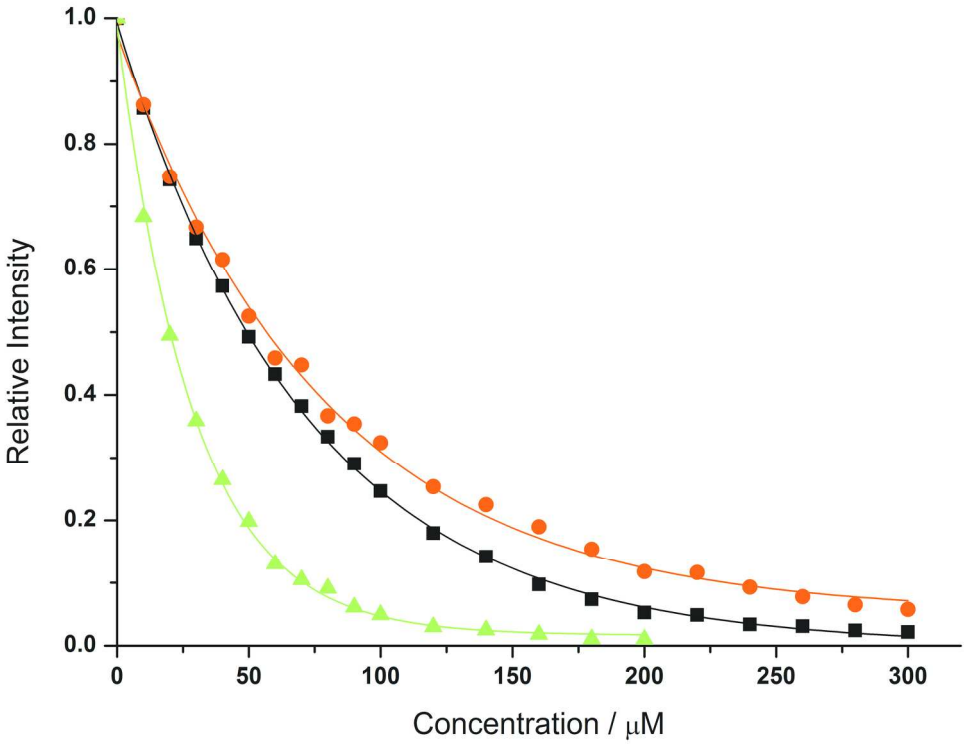

185x142mm (300 x 300 DPI)

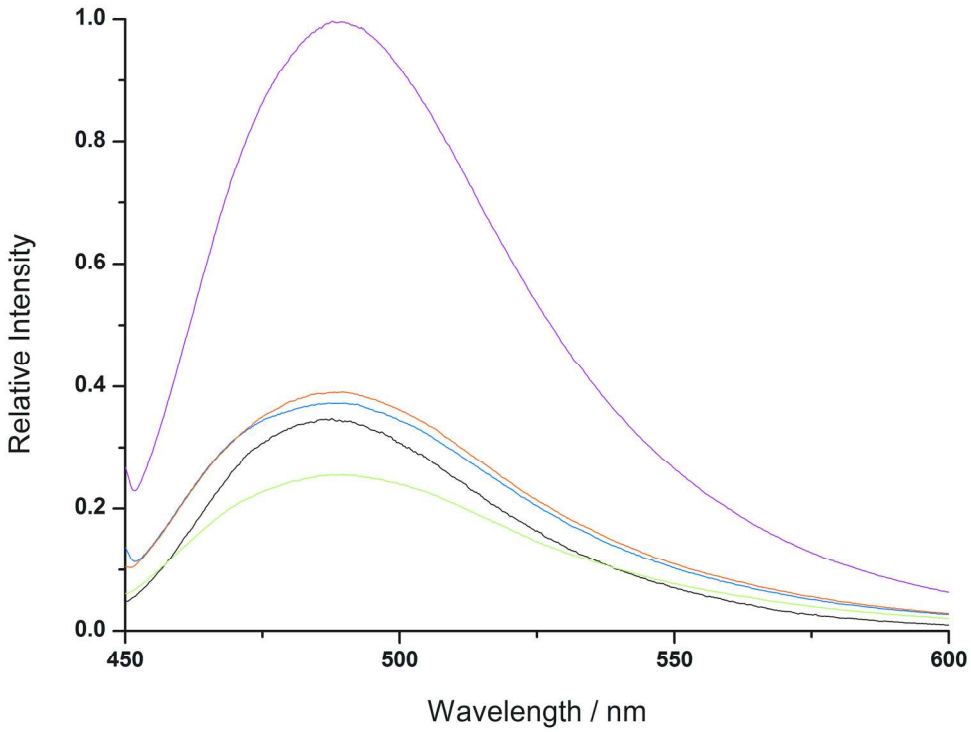

191x149mm (300 x 300 DPI)

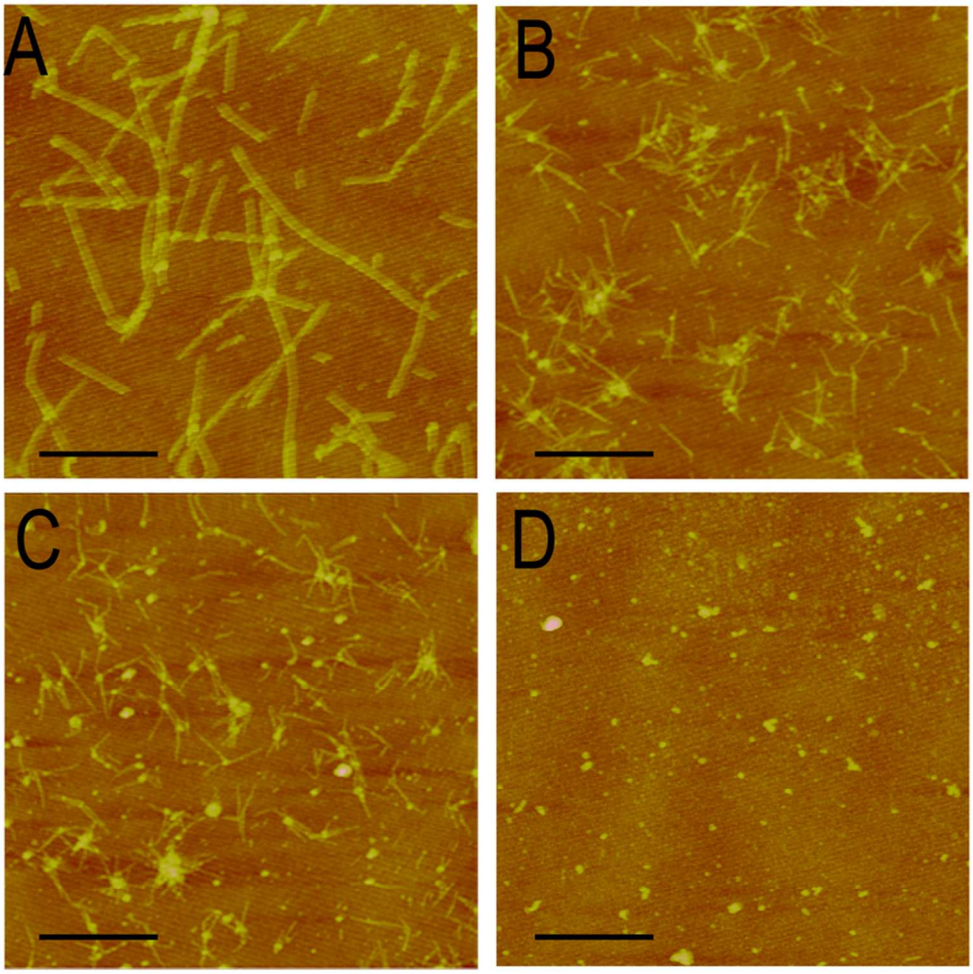

77x77mm (300 x 300 DPI)

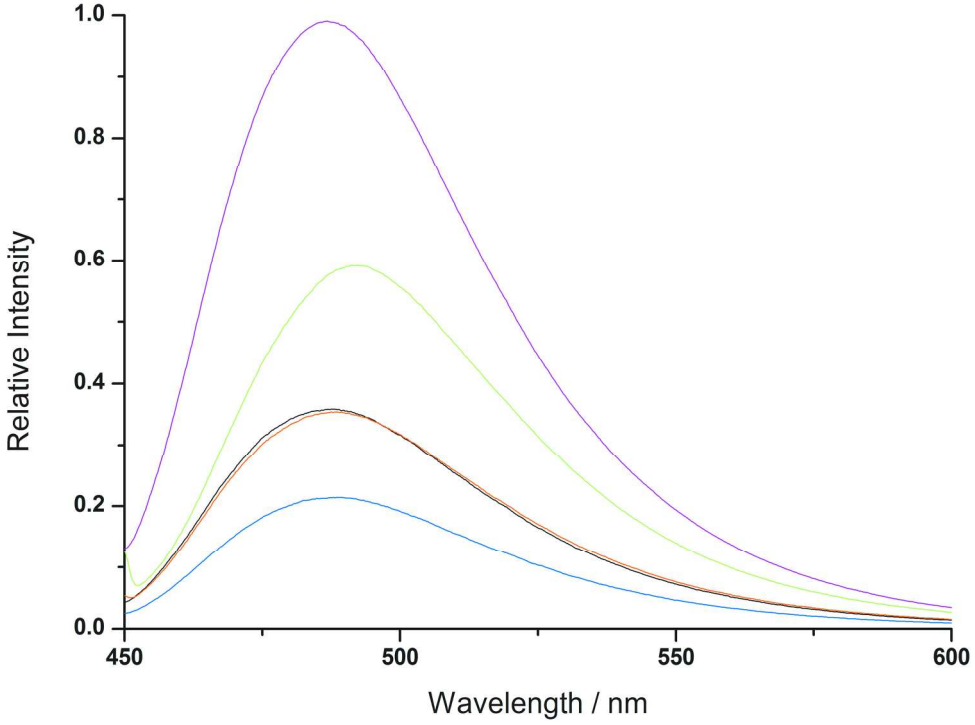

188x144mm (300 x 300 DPI)

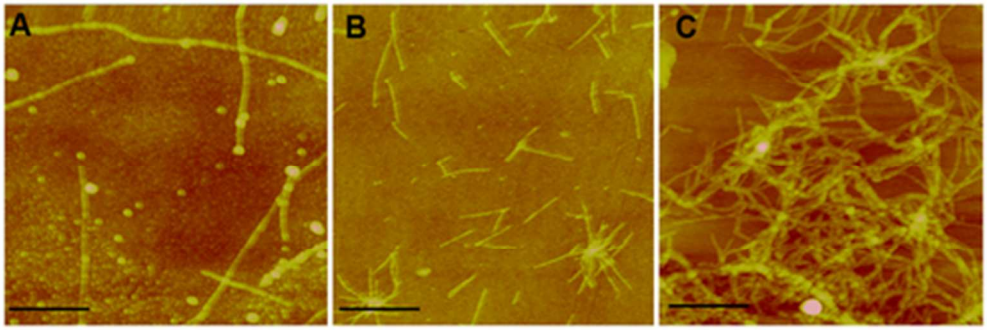

42x13mm (300 x 300 DPI)

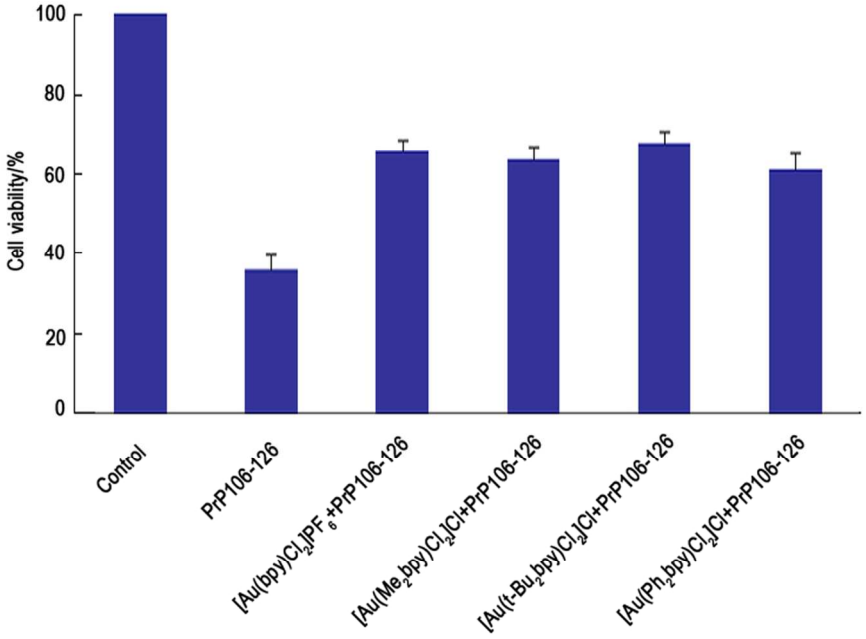

124x89mm (300 x 300 DPI)